Chapter 1

Introduction

Oxide compounds have shown immense potential in emerging fundamental science and engineering applications. Researchers are mainly focused on transition metal oxides (TMOs), rare-earth and alkaline elements due to their exceptional properties [1, 2]. TMOs have shown a remarkable degree of features due to the nature of the valence *d*-electrons, permitting the creation of distinct electronic correlations [3]. The oxides have a wide range of structures such as perovskites, spinel, garnet, hexaferrite, pyrochlore, *etc.*, based on their atomic arrangement in the unit cells. Perovskite oxides have exceptional properties induced through complicated interactions due to different kinds of charge, spin, & orbital orderings that correlate with lattice degrees of freedom. Different ordered parameters in association with defects will lead to a complex phase diagram [4]. The trend towards device shrinkage has highlighted the importance of multifunctional materials *i.e.*, materials that can do more than one task or multiple independent stimuli can control that.

Double perovskites are known to be multifunctional materials due to two different B-site cations, which make a complex arrangement in the different charge, spin, and orbital ordering that vary with composition, synthesis route, and conditions.

1.1 Perovskite

Perovskite materials can be described with a general structure of ABO_3 where A is an alkaline/rare earth element (Ba, Sr, Ca, La, Sm, Y, *etc.*), and B is a transition metal cation (Mn, Fe, Cr, Ti, Ni, Nb, Co, *etc.*). The perovskite structure is seen in Figure (1.1), with A cation at the corner and B ion present in the center of BO_6 octahedra [5]. The perovskite structure should have different sizes and valencies of A & B site cations. Materials with a crystal structure similar to calcium titanate ($CaTiO_3$) are known as perovskite materials.

Perovskite generally has a cubic lattice, although it deviates from that, as measured by the Goldschmidt tolerance factor (t) [6]:

$$t = \frac{r_A + r_O}{\sqrt{2}(r_B + r_O)} \tag{1.1}$$

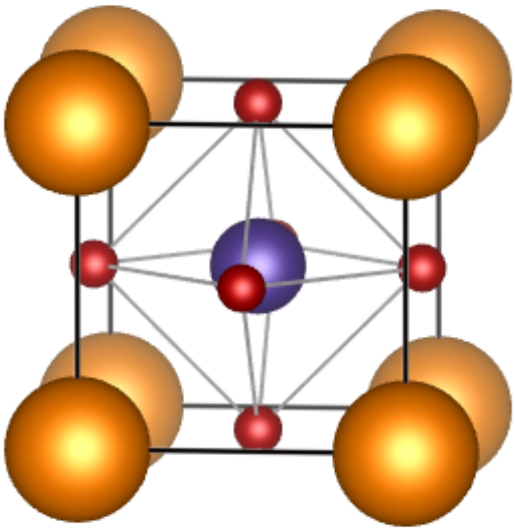

Fig. 1.1 Cubic unit cell where dark yellow, blue and maroon balls show A & B cations, and O anions, respectively.

where r_A, r_B, and r_O are radii of A, B, and O elements, respectively. The t values for various perovskite structures are in a range from 0.8 to 1.1, where t = 1 refers to a cubic structure [6]. For $t \neq 1$, there is a possibility of different structures such as orthorhombic, rhombohedral, tetragonal, *etc.*. Generally, perovskite structures have three different kinds of distortions/modifications, such as displacement of cations or distortions in octahedra (*e.g.* $BaTiO_3$) and tilting of an octahedral cage (*e.g.* $CaTiO_3$) or combination of both (*e.g.* $NaNbO_3$) [7–9]. The distortion in perovskites depends on A & B site cations, valence state, and oxygen vacancies in lattice [5, 7]. The properties (magnetodielectric, ferroelectric, piezoelectric, and magnetic) were extensively changed with distortion and chemical doping. Doping and substitution are possible on both the A and B sites of a perovskite structure depending on the various conditions [5, 7]. Thus, when half of the B sites are occupied in an orderly manner by two distinct cations (B and $B^{'}$) inside the structure, it becomes double perovskite [5, 10, 11].

1.2 Double Perovskite oxide

The typical formula for double perovskite (DP) is $A_2BB^{'}O_6$ or $AA^{'}BB^{'}O_6$ (where $A/A^{'}$ are rare-earth, alkaline, or alkali metals, and $B/B^{'}$ are transition metal ions) [5, 11, 12]. The unit cell is doubled, and perovskite units are alternated along distinct crystallographic directions. Transition metal ions combine with oxygen anion to generate two forms of octahedra, BO_6 and $B^{'}O_6$ [11, 12]. The octahedra's BO_6 and $B^{'}O_6$ ordered arrangement have three different possible configurations [11]. As shown in Figure (1.2) ordered configurations are rock-salt, layered, and columnar. The rock-salt structure has alternate positions of octahedra's and for layered or columnar has an alternating position of layers or columns of octahedra.

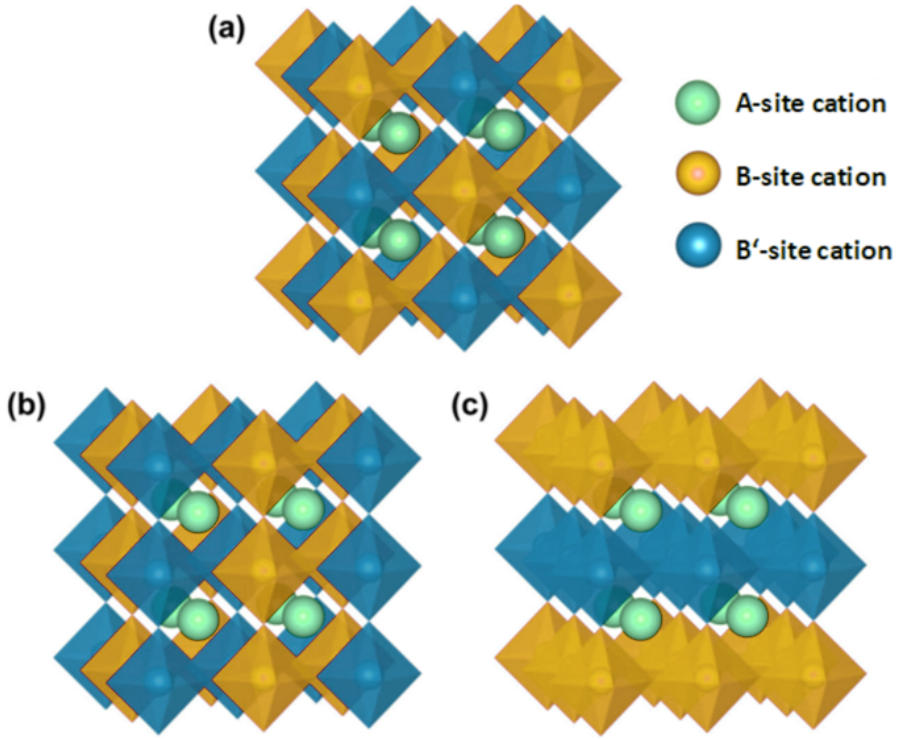

Fig. 1.2 Three different ordered distribution of octahedra in DP such as (a) rocksalt, (b) columnar, and (c) layered, here blue and yellow colour represents the BO_6 and $B^{'}O_6$ octahedra, respectively.

The cationic ordering of B and $B^{'}$ considerably influences the electronic and magnetic properties [13]. Double perovskites, based on various charge-cation combinations, have different properties. Figure (1.3) depicts the different B-site possibilities for a given A-site. Although it is challenging to synthesize all $A_2BB^{'}O_6$ at ambient pressure, most of it can be accomplished [11]. In particular, Ba_2CrTaO_6 formed a hexagonal structure at ambient pressure [14], DP phase in Ca_2InOsO_6 is synthesized at high pressure [15], and

La_2CuVO_6 formed a combination of La_2CuO_2 and $LaVO_4$ [16]. The unique properties of double perovskite arise from the various combinations of B and B$^{'}$. The different atomic combinations of A, B, and B$^{'}$ elements give rise to intriguing physical properties such as charge ordering [17], high-temperature spin ordering [18], half metallicity [19], ferroelectricity [20], and giant dielectric constant [21]. In the case of double perovskites tolerance factor (t) is represented as

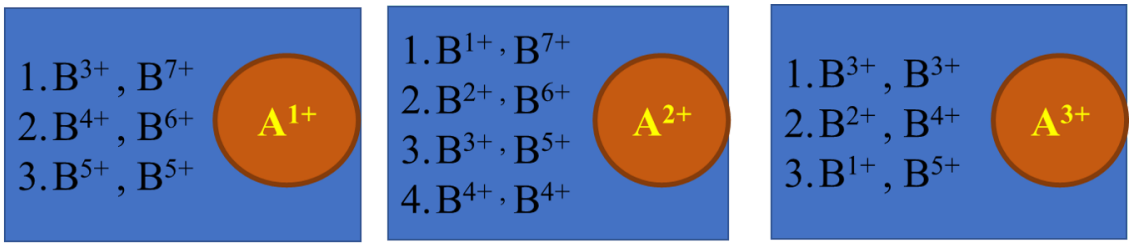

Fig. 1.3 Possible combination of different charge valence cations A, B, and B$^{'}$ in double perovskite.

$$t = \frac{((r_{A'} + r_A)/2) + r_O}{\sqrt{2}((r_{B'} + r_B)/2) + r_0} \tag{1.2}$$

where r_A, r_B, $r_{A'}$, and $r_{B'}$ are the ionic radii of A, B, A$^{'}$, and B$^{'}$ cations, respectively, r_O is the radius of oxygen anion. Octahedra distortion or tilting and cationic displacement are frequent in these compounds due to the different ionic radii of cations at the A and B sites. The distortion in unit cells can be explained by geometric factors [11]. Distortion as well as cationic disorders, are prominent features in these types of systems. When two BO_6 octahedra are aligned in a regular periodic fashion throughout the unit cell, the unit cell is said to be ordered; otherwise, the unit cell is referred to as disordered [11, 12].

Disorders in double perovskites are classified into two types: antisite disorder (ASD), and antiphase boundary (APB) are shown in Figure (1.4). Due to configurational entropy, such point-like AS defects are mostly expected to be present where B and B$^{'}$ cations interchange their locations. Another common type of defect is the APB, which separates two ordered domains with reversed B and B$^{'}$ site occupancies and can be considered as an accumulation of antisites. The presence of vacancies and different B-cations induces distortion in the unit cell that affects the bond-length and bond angle between the cation and anion. The magnetic interaction between cations, electrical, optical, and other properties varies from ordered to disordered phase. The valency of B and B$^{'}$ also differs due to heat treatment during the synthesis and hoping of electrons through oxygen vacancies.

The disorder or antisites impact the saturation magnetization, magnetoresistance, electric conductivity & resistivity, and electronic band structure [11, 12, 22–26].

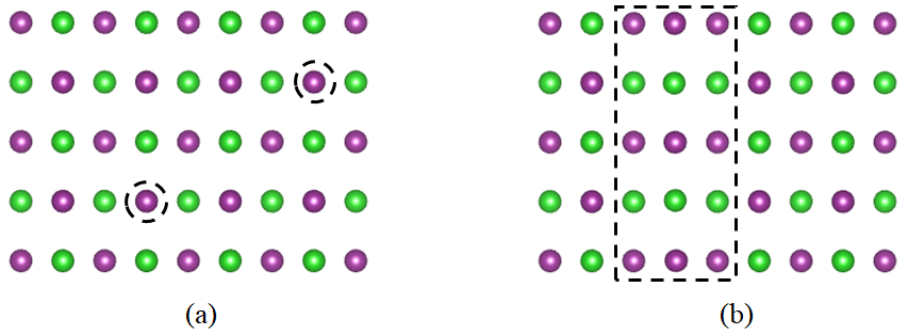

Fig. 1.4 Octahedra disorder (a) antisites defects, (b) antiphase boundary (APB), where green and purple circle represents as an octahedra.

The B-site cations ordering depend on charge and size difference. The difference in the B and $B^{'}$ cation oxidation states, $Z_B = Z_{B}^{'} - Z_B$, is widely considered as the fundamental cause producing B-site cation order in these compounds. In general, when Z_B is less than 2, the compounds are disordered, and when Z_B is greater than 2, the compounds are ordered [11, 13, 27]. When Z_B is big, placing two highly charged B cations next to one other is energetically unfavorable relative to the ordered arrangement. As noted, in the situation of $Z_B = 2$, a large range of degree of order is generally feasible, and in these cases, numerous other contributions affect the cation ordering. Synthesis conditions, particularly synthesis temperature, are among the most critical. The ordering has a big impact on magnetic, electric, and other properties [19, 23], and the best properties are generally found with a lot of order. The ionic radius differential, $r_B = r_{B'} - r_B$, is a second well-known component that influences cation order. The greater the disparity, the more likely the order is. Increased lattice strain overcomes entropic considerations when the difference in ionic radii is high enough, and the cations are ordered. In a small number of compounds with M^{3+}/Nb^{5+} cation combinations at B-sites, Galasso and Darby [22] investigated the influence of ionic radius difference on ordering. Their findings suggested that a radii difference of more than 7-17 % would be sufficient to cause order.

1.3 Distinction of perovskites and double perovskites

In the last 20 years, researchers have focused on exploring perovskite families due to the versatility of applications. The double perovskites have thermionically stable compounds, and their applications in a different areas of fields such as in LED ($Cs_2AgInCl_6$), LASER

(Cs_2NaGaF_6), superconductors (La_2CuSnO_6), multiferroic (Bi_2NiMnO_6) and even in X-ray imaging ($Cs_2AgBiBr_6$) [24]. The double perovskites have two B-site cations that provide flexibility and tunability of properties as compared to perovskites. Controlling B and $B^{'}$ structural ordering may therefore aid in the linkage of their functional properties [25, 26]. The double perovskites have an ordered and disordered phase that modified the magnetic exchange interactions, electronic band structure and band overlapping. The presence of the order and disorder phase makes them a suitable candidate for inducing magnetic frustration in the system.

The double perovskites are also favorable due to the presence of charge ordering and as well as spin and orbital ordering [17, 28]. The different ordering makes complex scenarios to explain the overall magnetic behavior of these systems. These types of compounds also show a half-metallic nature and metal-insulator transition [19, 29]. The short and long-range magnetic ordering, unusual spin-orbital coupling (SOC), and better electronic and dielectric properties are key advantages of double perovskites.

1.4 Magnetic interaction

The exchange interaction of a spin with its surrounding determines the magnetism of materials. Spins interact with their nearest neighbors (NN), next-nearest neighbors (NNN), and n^{th} neighbors, depending on the crystal structure. As two metal ions or spin interact directly then it is known as a direct exchange interaction, and if the interaction mediates by nonmagnetic (oxygen) anion then an indirect exchange interaction. In the case of oxide perovskites, various indirect exchange interactions such as super-exchange, double exchange, *etc.* will be discussed.

1.4.1 Superexchange interaction

Superexchange interactions in oxides occur between two magnetic cations mediated by an oxygen anion with a semi-covalent bond. According to the second-order perturbation theory, the superexchange interaction is highly influenced by the metal-oxygen–metal (M-O-M) bond angle. When M-O-M bond angle is nearly equal to 180° or spins are colinear then antiferromagnetic coupling strength is higher, and the tendency of ferromagnetic alignment when M-O-M bond angle is 90° but smaller than the previous. Therefore, different configurations and orientations of *d*-orbitals have ferro/antiferromagnetic types of superexchange interactions.

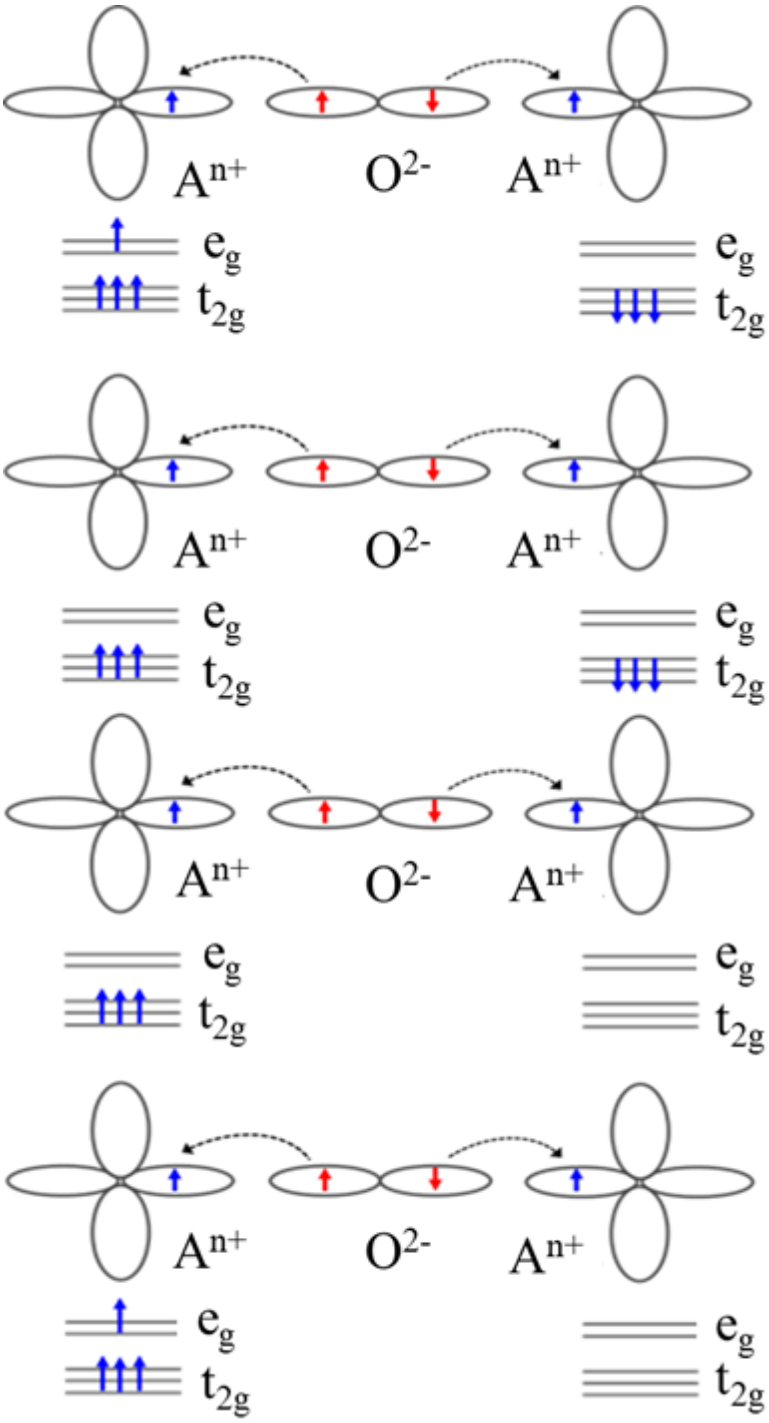

Fig. 1.5 Different types of superexchange interactions, between filled, half filled, and vacant orbit.

The interaction between two magnetic cations is either ferromagnetic or antiferromagnetic and mediated by a non-magnetic or oxygen anion. Pauli exclusion principle favours to antiparallel spin configuration for two electrons in same e_g, while the Hund rule forces

parallel spin arrangement of electrons with in different d-obits (e_g-t_{2g}) of same 3d shell [30]. A schematic diagram of ferro/antiferromagnetic superexchange interaction between different configurations of filled, half-filled, and vacant d orbitals are shown in Figure (1.5(a)). The interaction of a fully filled d orbital with a half-filled d orbital results in ferromagnetism, whereas two half-filled d orbits interact with antiferromagnetic nature. (b) When a half or full filled orbital interacts with an empty orbital, the outcome can be antiferromagnetic or ferromagnetic although, in most situations, ferromagnetic nature is preferred. In case of La_2NiMnO_6 ferromagnetic superexchange interactions occur between Ni^{2+}-O^{2-}-Mn^{4+} (e^2-2p-e^0) cations whereas antiferromagnetic superexchange interaction between Ni^{2+}-O^{2-}-Ni^{2+} (e^2-2p-e^2) or Mn^{4+}-O^{2-}-Mn^{4+} (e^0-2p-e^0) cations [31].

1.4.2 Double exchange interaction

Double exchange interaction arises between different charge valences of magnetic cations, proposed by Zener [32]. Double exchange interaction occurs in a mixed phase or multiple valences in a compound. The presence of multiple charge valences and charge transfers are common in double perovskite oxide compounds that makes them suitable candidates for this type of interaction. According to Zener [32], induced ferromagnetism is caused by the double exchange interaction between magnetic cations of different oxidation states linked via oxygen anion because electron spin remains unchanged during the transfer of electrons.

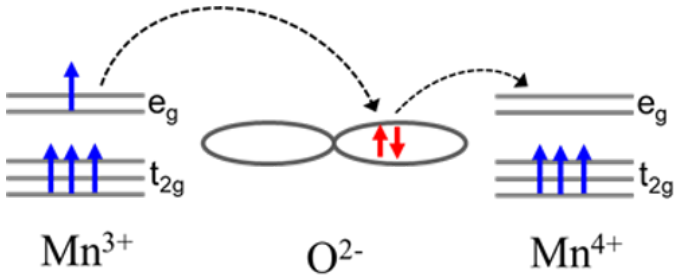

Fig. 1.6 Double exchange interaction mediated through oxygen ion.

The FM originates in such systems is governed by the double exchange (DE) mechanism and can be understood considering Figure (1.6). FM arrangement of neighboring ions is required to retain the high-spin arrangement of both the receiving and the donating ions. This model is alike to superexchange. In superexchange, an AFM or an FM alignment takes place among two atoms having the same number of electrons (valence), while in

double exchange; the interaction takes place only when one atom has an extra number of electrons compared to the other.

1.4.3 Crystal field splitting

The crystal field is an electric field generated by the crystal's surrounding atoms. The adjacent orbitals are treated as negative point charges in crystal field theory (CFT). The most advanced systematic work on this approximation is ligand field theory, which effectively enhances molecular orbital theory by showing important properties of *d* orbitals on the core cation that overlap with surrounding orbitals of adjacent anions (ligands). Crystalline field theory focuses on the interaction of *d* orbitals of central ion (in transition metal for perovskite structure) and donor atoms of ligands. As a result, the crystal field highlights the energy division caused by the *p-d* hybridization of transition metal ions and O atoms. The crystal field theory [33] shows localized d-orbitals and how it interacts with spin, orbital, and lattice degrees of freedom. The Hund interaction will give two different energy bands in transition metals with spin up (↑) and down (↓) for each band.

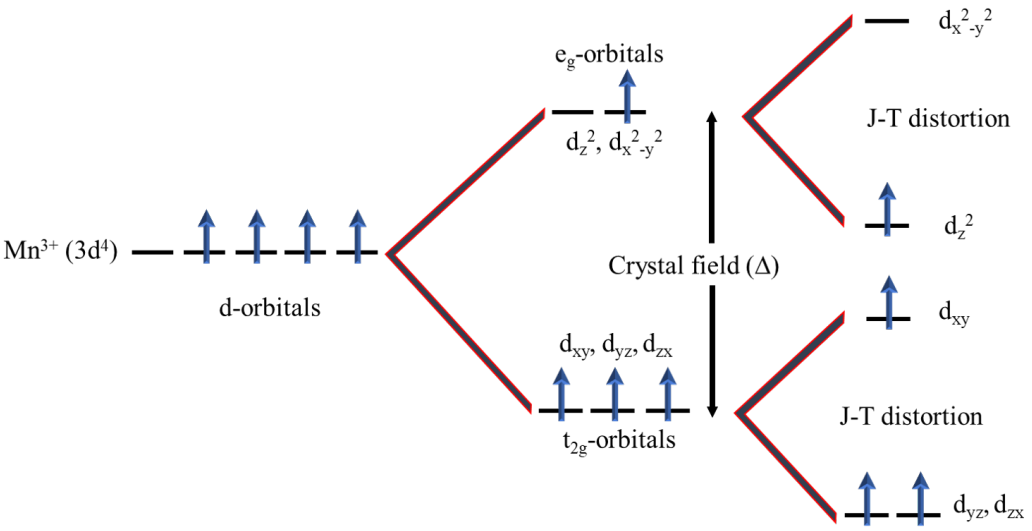

Fig. 1.7 Crystal field splitting and Jahn-Teller distortion in Mn^{3+} cations, arrow indicates the spin up (↑) & down (↓) configuration.

Taking example of manganite , the core transition metal Mn accompanied by oxygen ions, crystal field breaks *d*-orbitals degeneracy due to Coulomb repulsion with the O^{2-} ligands [33]. The d orbits of a transition metal ion split into two groups: the e_g doublet ($d_{x^2-y^2}$ and d_{z^2} orbitals), lying higher in energy, and the t_{2g} triplet (d_{xy}, d_{yz}, and d_{zx} orbitals)

which are lower in energy as shown Figure (1.7). Since e_g doublet points directly towards the O atoms and hence feel a more electrostatic repulsion from the O electrons and t_{2g} triplet away from the O atoms so repulsion is comparatively less [34]. The amount of splitting (Δ) is influenced by parameters such as ion repulsion, octahedron shape, and the effects of Jahn-Teller (J-T) distortion. The J-T effect is sensitive to partially occupied e_g states, which is caused by reducing the electronic energy through distortion of BO_6 octahedra [35]. In the case of Mn^{3+} (t_{2g}^3 e_g^1) ion, the presence of the doubly degenerate e_g levels, the octahedron is distorted to remove the degeneracy of the levels. To remove the degeneracy, the O ions which are around the Mn^{3+} ions readjust their location to create an asymmetry in different directions (see Fig. (1.7)). The octahedron MnO_6 is distorted as there are long and short Mn-O bonds appear. In R_2NiMnO_6, Jahn-Teller ions have a single electron in a two fold-Mn degenerate fluctuating e_g-orbital occupation, as in $Ni^{3+}(e^1)$-O^{2-}-$Mn^{3+}(e^1)$, $Mn^{3+}(e^1)$-O^{2-}-$Mn^{3+}(e^1)$, and $Ni^{3+}(e^1)$- O^{2-}-$Ni^{3+}(e^1)$, resulting in a three-dimensional ferromagnetic vibrionic superexchange interaction [36].

1.5 Magnetism in double perovskite

Magnetism in DP is due to the presence of magnetic interaction (double exchange and superexchange) between the large combination of B and B$^{'}$ cations. Mostly double perovskites have ferromagnetic, antiferromagnetic and spin glass nature on the basis of interaction between different B-site cations. Apart from this magnetic phase, DP can be superconducting, metallic and insulating. Following section presents the discussion from a ferromagnetic insulating phase.

1.5.1 Ferromagnetic insulating nature

Modern electronic and spintronic devices' basic need is less dissipation which is possible by using ferromagnetic insulators (FMIs). The insulating nature is an important property for modern device applications that will encourage researchers to work on double perovskites. The crystal field spilting of *d* state is due to presence of different B and B$^{'}$ in BO_6 and B$^{'}$O$_6$ octahedral site. This will leads to crystal field spliting of *d*-state of B and B$^{'}$ into t_{2g} and e_g. A distortion in bond angle in oxide DP materials leads a reduction in effective *d*-electron hopping energy due to lower hybridization between transition-metal *d* and oxygen *p* states, resulting in an insulating state. The developing FMI state caused by cation manipulation in these materials provides the path for the creation of novel oxide quantum materials and spintronic devices. Due to the unusual mechanism of their ferromagnetism,

which derives from the hybridization mechanism rather than the RKKY interaction. DP materials containing both *3d* and *5d* transition metal ions are intriguing candidates for FMIs. High-temperature ferromagnetism is stabilized in this mechanism by a substantial exchange splitting of one of the two magnetic ions.

1.5.2 Antiferromagnetic insulating nature

Double perovskites show antiferromagnetic (AFM) characters for some combination of B and B$^{'}$. The AFM ordering is common in compounds with a combination of R and *4d*/*5d* element at B and B$^{'}$ (type-2 or A-type), and or both B-site cations are transition metals (type-1). In type-1 AFM is due to these *3d* elements having electrons on the e_g orbitals, allowing for σ-interactions, which would enhance the 180° next nearing neighbor (NNN) coupling. Other A or type-2 has empty e_g orbitals, resulting only ϕ-interactions, with strong 90° nearest neighbor (NN) coupling.

1.5.3 Ferromagnetic metallic nature

In terms of the electronic configuration of B and B$^{'}$, ferromagnetic double perovskites might exist. Very few of the DP are reported to be metallic, which shows either borderline metallic behavior or metal-insulator transitions (MIT).The electronic bandwidth of DP materials is significantly influenced by the spatial overlap between the orbitals of different elements. The contracted nature of the *3d* orbitals results in weak overlap with the O-*2p* orbitals, particularly in the case of ϕ-bonds, when *3d* transition metal elements are present at the B-site. On the other hand, the *4d/5d* orbitals are typically more extended, resulting in wider bandwidths when *4d/5d* transition metal cations are present at the B-site. Therefore, spin delocalization is more prevalent in DP materials containing *4d/5d* elements. In reality, the compound under investigation were either metallic or nearly metallic.

1.5.4 Spin-glass nature

The spin-glass phase stablized in a system broadly either due to large B-site disorder (as in Sr_2FeCoO_6 [37]) or due to geometric frustration (as in Ba_2YMoO_6 [38]). If B-site cations are randomly occupied or different valence states distribute random positions then its known as antisites. This antisite arises in DP due to differences in ionic radii of B site cations. The interaction between two B-site intermediates by oxygen anion is either ferromagnetic or antiferromagnetic. Random distributed B-site cations will cause a race between NN and NNN interactions which will rise to spin-glass nature. The two different

B-site (*3d* and *5d*) have different ionic radii that lead to distortion in the unit cell. In DP two octahedra BO_6 and $B^{'}O_6$ are connected to each other, due to different B sites leads different size of octahedra. This arrangement is geometrically frustrated, which in conjunction with quantum fluctuations gives rise to spin-glass behavior.

Spin-glass characteristics

Disorder (randomness) or geometric frustration cause the spin-glass state. Magnetic frustration in the lattice is caused by the struggle between NN and NNN superexchange interactions, which is governed by the random distribution of cations. If all neighbors interact in a ferromagnetic manner, then it is non-frustrated. However, cation disorder alters the antiferromagnetic neighbor interactions, resulting in a number of degenerate ground states. Ruderman-Kittel-Kasuya-Yosida (RKKY) interaction describes the interaction between localized moments and conduction electrons [39]. It is long-ranged oscillatory in nature. It has a dependence on the distance between magnetic moments, and reduces drastically with the inverse of the third power of the r [39].

$$J_{RKKY} \propto \frac{Cos(2K_F r)}{r^3} \tag{1.3}$$

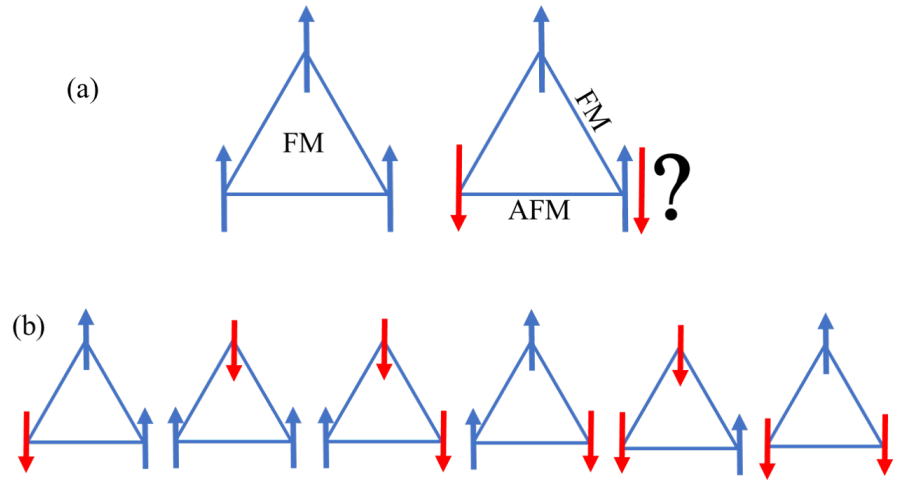

Fig. 1.8 (a) Degeneracy for a triangular lattice, (b) possible ground state for degenerated triangular lattice.

where, k_F is the Fermi wave-vector. The following Figure (1.8) shows a spin arrangement for a triangular spin-lattice. If two spins are arranged in an FM manner then the third is also in the same order but if two are in an AFM manner then third spin have the

probability of either FM or AFM leading to multiple ground state also known degeneracy of the system. The spin-glass nature is characterized by various approaches.

(a) Irreversibility of the system had been seen under dc-magnetization measurements. It was measured under zero field-cooled (ZFC) and field-cooled (FC) conditions. For spin-glass (SG), cluster glass (CG), & superparamagnetic (SPM) nature, ZFC and FC show different paths below irreversibility temperature (T_{irr}) (see Figure (1.9)). In ZFC mode, it shows a peak (cusp) at spin-glass freezing temperature (T_f) while in FC its shows a plateau below T_f. So the bifurcation in M-T curve, ZFC/FC protocol suggests the possibility of SG, CG and SPM nature.

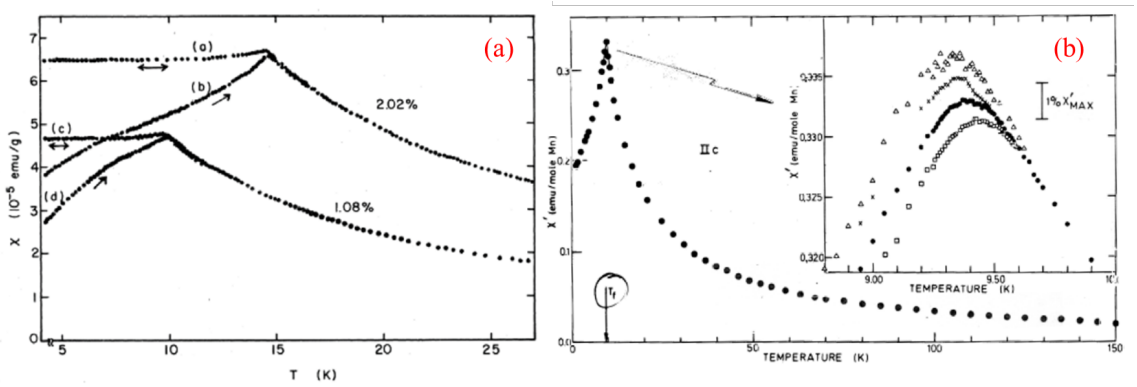

Fig. 1.9 (a) FC and ZFC of dc-susceptibility for CuMn alloy at 6 Oe field (Nagata *et al.* (1979)), (b) Real part of ac-susceptibility versus T for CuMn; inset expanded view of SG cusp near T_f (Mudler *et al.* (1981)).

(b) In ac-susceptibility measurement, a peak (cusp) occurs and shifted with frequency. The cusp shifted with frequency also suggests the possibility of SG, CG, and SPM. The cusp shifting defines the nature of the glassy system. The spins are frozen in a random direction below spin-glass freezing temperature (T_f) and by changing ac frequency changes the time of freezing that affect the surrounding interaction. The Mydosh parameter was utilized to differentiate between glassy nature and SPM [39]. For CG/SG systems value of the Mydosh parameter range from 0.3 to 0.005, whereas for SPM lies in the range of 0.1-0.3 [39]. The dynamics of spins are described by the relaxation time and relaxation mechanism. The relaxation time disclosed by the various formulism such as Vogel-Fulcher Law, Power-Law, and the relaxation mechanism (single or polydispersed) by the Cole-Cole formalism [39–42]. The relaxation time utilized to differentiate SG and CG, CG has faster spin dynamics while SG slow dynamics.

(c) the Taylor series expansion of magnetization at low field value gives linear and non-linear susceptibility (χ^2, χ^3....) terms that are also characteristic of spin glasses. The third harmonic of ac susceptibility (χ^3) is proportional to the negative sign of spin-glass

susceptibility and diverges at the spin-glass transition temperature (T_{SG}), evident of SG/CG kind nature [39, 43].

(d) SG/CG states of diluted and concentrated systems are characterized by criteria of slow dynamics, aging, and memory & rejuvenation effects. At low field value, SG/CG states are characterized by memory and rejuvenation effects that depend on time and temperature. The origin of SG/CG states is still being investigated or discussed. For memory and rejuvenation effect, droplet and hierarchical model-based protocols are utilized to characterize the nature of spin in the SG/CG state. The slow relaxation of magnetization in the SG/CG states follows a stretched exponential behavior where magnetization decay is measured as a function of time. [39, 40, 42, 44–47].

(e) The magnetic contribution to specific heat (C_m) is another criterion used to characterize the SG/CG states. The temperature dependence of C_m exhibits large maxima above the spin-glass freezing temperature (T_f) and linear behavior below this temperature. A two-level tunneling model is used to explain the linear character of C_m below T_f [10, 39].

1.6 Frustration mediated phenomena in double perovskite

Magnetic frustration is a phenomenon that occurs when an ordered to disordered phase transitions take place as a result of competing FM and AFM exchange interactions. Magnetic frustration in systems is typically caused by antiferromagnetic or a combination of ferro/antiferromagnetic magnetic interaction. The geometry of magnetic ions, such as a triangular lattice (discussed in the spin-glass section), also caused frustration. Magnetic frustration causes the system to exhibit complex magnetic behavior such as spin-glass, spin liquid, spin ice, and so on. Because of the presence of an order/disorder phase, double perovskites are the best compounds for these types of features. The cation ordering phase (Ni-O-Mn) generates FM ordering in the R_2NiMnO_6 compounds, while the disordered phase (Ni-O-Ni, Mn-O-Mn) generates AFM order. Because of the presence of FM/AFM ordering and its competitive nature, the chemical structure is suited for glassy dynamics. The spin-glass and its features have already been described. The FM/AFM interface stabilized the exchange bias in the systems. The existence of both ordered and disordered phases in a double perovskite compound may signify the exchange bias and glassy nature.

The spin-glass state that is still being debated is the aging, memory, and rejuvenation effects as a function of time (t) and temperature (T) [44, 45]. The observed effects in the spin-glass state have been described using the droplet [46] and hierarchical [47] approaches. According to the droplet model [46] of the spin-glass phase, there is a characteristic two valleyed free energy landscape associated by global spin reversal corresponding to each

temperature below the T_{SG}. In the hierarchical [47] model, on the other hand, the free energy landscape is multi-valley at all temperatures below T_{SG}, with valleys splitting into new sub valleys as temperature decreases and merging as temperature increases. The protocols for both models are described in a following chapters.

1.6.1 Exchange Bias

The exchange bias effect is a decade of phenomena discovered by Meiklejohn and Bean in 1956 [48]. They discovered a field-cooled hysteresis loop in partially oxidized Co particles that are shifted along the magnetic field axis. This behavior is attributed to the exchange interaction at the interface between the ferromagnetic Co core and the antiferromagnetic CoO shell [48]. The exchange bias arises due to the presence of competing FM and AFM exchange interactions and a rise in unidirectional anisotropy which provides additional remanence. The interface of FM and AFM layers generates exchange bias *via* hysteresis loop shifting when the AFM layer is uncompensated or when the AFM layer has compensated spin then the loop is broadened. In recent development, exchange bias has been divided into two major categories: conventional and spontaneous. The shift in the hysteresis loop under field cooling is termed a conventional exchange bias (CEB) phenomenon, whereas it is considered a spontaneous exchange bias (SEB) phenomenon under zero-field cooling [49, 50]. The exchange bias field ($H_{CEB/SEB}$) can be computed from the hysteresis loop shift as $H_{CEB/SEB} = (H_{c1} + H_{c2})/2$, where H_{c1} and H_{c2} are the coercive fields associated with the descending and ascending branches of the hysteresis loop, respectively [48–50]. The sign of $H_{CEB/SEB}$ could be positive or negative depending on the shift direction along the field axis.

The exchange interaction formed at the ferromagnetic/antiferromagnetic interface is a fundamental physical phenomenon, because antiferromagnets have minimal or no net magnetization, an external magnetic field has only a minor effect on their spin orientation. During magnetization reversal, the antiferromagnet spin order is conserved. The energy required to overcome the interfacial exchange coupling will now constrain the reversal of the ferromagnet's moment. This additional energy term suggests a shift in the ferromagnetic film's magnetic hysteresis from zero magnetic fields. Thus, the magnetization curve of an exchange-biased ferromagnetic film is moved away from zero magnetic fields by an amount of exchange bias field H_{EB}, and coercivity is increased [51]. Recently, EB effects are seen in a mix of hard and soft FM layered systems, either directly through exchange coupling or indirectly via a nonmagnetic interlayer. Coupling is proposed in the latter situation to result through dipolar and RKKY interactions. The exchange bias is also

induced in core-shell structures where surface anisotropy or complex mechanisms are at different interfaces.

1.7 Literature survey and background of La_2NiMnO_6

La_2NiMnO_6 (LNMO) is a most studied of double perovskite oxide ($A_2BB^{'}O_6$), that mainly presence of various interesting physical, magnetic, electronic, and optical properties. The connection of electric, magnetic, and lattice degrees of freedom results in these properties [52]. This makes the material appealing for fundamental research as well as spintronic device applications such as magneto dielectric capacitors, spin-based sensors, multiple state memory elements, spin tunneling junctions and gas sensors, solar cells, electric tunable devices, and so on.

1.7.1 Crystal structure

The crystal structure of double perovskite depends on B and $B^{'}$ cations ordering which depends on the synthesis route, calcination, sintering temperature, and calcination atmosphere. The ordering of Mn^{4+} and Ni^{2+} changes their crystal structure from orthorhombic (P*bnm* space group) to monoclinic ($P2_1/n$ space group) [53]. The initial report on LNMO suggests the orthorhombic structure [54]. Further researchers identified other crystal structures or mixed structures. Sometimes biphasic (rhombohedral and monoclinic phases) compositions are reported which is also proven by neutron diffraction [55]. D. Yang *et al.* [56] defined that with the heating and vacancies, monoclinic phase converts into rhombohedral which regains the monoclinic phase with cooling and pressure variation. The high-temperature phase of LNMO is cubic which is Rock-salt cations (octahedral) arrangement [56]. The following table describes the different phases of LNMO with varying synthesis routes and temperatures.

It has been detected that monoclinic and rhombohedral phase have ordered cations arrangement while disordered distribution have an orthorhombic phase. The disordered phase has either random distribution of Ni and Mn cations or surrounded by different valence state. It is difficult to define the cations distribution or crystal structure for case of LNMO through X-ray diffraction (XRD) due to nearly similar ionic radii or electronic distribution. The distribution of Ni/Mn play a vital role in local crystal structure and distortion (bond-length and angle) which affect the electronic and magnetic nature of LNMO. Thus, a close relation is seen between disorder (AS and APB) and magnetism.

Table 1.1 Crystallographic data (crystal structure and lattice parameter) with different synthesis conditions.

Synthesis	Condition	Space group	a (Å)	b (Å)	c (Å)	β (°)	Ref.
Pechini method	1350 K, 6 h, air	$P2_1/n$	5.517	7.748	5.466	90.01	[53]
Sol-gel method	1673 K, 12 h, air	42 %, R3c 58 %, Pbnm	5.504 5.503	- 5.452	13.235 7.727	-	[57]
Sol-gel method	1273 K, 12 h, Ar	32 %, R3c 68 %, Pbnm	5.512 5.512	- 5.458	13.236 7.739	-	[57]
Solid state reaction	1573 K, 4d, air	Pbnm	5.477	5.464	7.670	-	[58]
Modified nitrate route	1373 K, 16 h, Air	$P2_1/n$	5.467	5.510	7.751	90.12	[59]
Sol-gel route	723 K, 6 h	R3c	5.4952	-	13.3558	-	[60]

The different structures and phase fractions have different electric, optical, and magnetic properties [53–60].

1.7.2 Magnetism

First principle density functional theory (DFT) computations employing the full potential linearized augmented plane wave (FP-LAPW) technique validated the ground state ferromagnetic nature [31]. The magnetic nature of LNMO depends on the presence of charge valence & it's distributions and oxygen vacancies. The spin-polarized calculations confirmed the observed magnetic moment in this compound is 5 μ_B per formula unit [12, 26, 31, 53]. The magnetic moment value meets the conditions for the Hund's first rule moments Mn^{4+} ($3d^3$) ; t_{2g}^3 e_g^0 and Ni^{2+} (d^8) ; t_{2g}^6 e_g^2 that confirming Goodenough–Kanamori (GK) rule that the coupling between the nearby Mn^{4+} and Ni^{2+} ions are ferromagnetic in nature. Depending on charge ordering/disordering, the magnetic nature of LNMO is classified into the following categories. (a) The long-range of Ni/Mn ordered cations shows a single transition, paramagnetic to ferromagnetic at $T_c \sim 280$ K from ferromagnetic superexchange interactions of Ni^{2+}-O^{2-}-Mn^{4+} [26]. (b) An admixture of ordered and disordered Ni/Mn cation distributions shows multiples transition. Several studies have yet to resolve the appearance of the low-temperature transition (≤ 150 K) [12, 26, 61–63]. In other research, magnetic transitions at lower temperatures $T_{c2} \sim 150$ K were described as antiferromagnetic transitions due to antisites or charge disorder [26]. The low-temperature transitions in LNMO have also been ascribed to a second ferromagnetic ordering related to the Ni^{3+} (Mn^{3+}) cations [62, 63]. According to Gauvin-Ndiaye *et al.* [64] Jahn-Teller ions (Ni^{3+} & Mn^{3+}) are formed during electron transfer of oxygen anion to Ni^{2+} & Mn^{4+}, while other study defines an inhomogeneous system (based on

the presence of different chemical valence state) formed during heat treatment [65]. It is difficult to the identified different charge ordering and exchange interactions. In the case of thin-film various techniques utilizes to probe the charge transfer at the interface of Ni and Mn octahedra, while in the case of crystallite or bulk, charge transfer is still not reported.

Zhu *et al.* [66] investigated the magnetic and electronic properties of La_2NiMnO_6 with Ni/Mn ordering in (111), (110), and (001) directions using first-principles electronic structure computation. Because the presence of ferromagnetic and antiferromagnetic interactions and their competing nature make them suitable candidates for exchange bias spin glasses and magnetic/spin frustration. The spin glasses were reported by various researchers below 100 K [26, 63]. The T_c, T_{SG}, and spin dynamics are varying with particle size, the fraction of antisites disorder, cation & anion vacancies in the samples. The ferromagnetic T_c's close proximity to room temperature makes it an appealing candidate for spintronics applications. Antiphase barriers are also present in the LNMO highly ordered sample [53]. At zero field, the antiphase boundary connects the adjacent ferromagnetic domains antiferromagnetically, but a tiny applied field is capable of rotating the ferromagnetic domains with a 360° spin rotation across the antiphase borders, resulting in little remanence in the hysteresis loop [53].

1.7.3 Impact of doping

Doping has shown considerable effect on the properties of parent double perovkites compounds. Doping or chemical substitutions are performed by either electron/hole doping (reduced valence) or element substitution with another element with a lower/higher ionic radius of the same valency. The double perovskite has different A & B sites, and the researcher replaced cations to see the effect on their properties. The elemental substitution at A or B sites will affect the lattice parameters and tilting & distortions of octahedra as well as impact antisites and APB. The tilting and distortion of octahedra affect the bond-length (Ni/Mn-O) and the bond angle (Ni(Mn)-O-Mn(Ni)) which modify the magnetic transition and magnetic exchange interaction. The substitution of other lanthanide elements at the La-site results in a decrease in unit cell volume due to reduced ionic radii [67]. FM T_c likewise decreases from 287 K to 40 K when one moves from La to Lu in the series [67–69]. Researchers use a small amount of alkali earth metal replaced with La in LNMO, which affects the magnetic nature as well photocatalytic and optical properties [63, 70].

The band gap also increases with the substitution of lower ionic lanthanides [68, 69]. The doping or chemical substitution affects the bond angle and length due to the distortion and tilting of octahedra. In the case of Cu doping, Cu-Cu length influences the overlapping of the electronics band. In case of Cu doped in $Cs_2SbAgCl_6$ decreases the bond-length

from 2.6 to 1 eV [71]. The Cu doping influence the electronic band, and interactions of octahedra with the Cu-O layer manifests the superconductivity in the system. The electron and hole doping provide free electron/holes which influences the conductivity of the system and can be used as a solid oxide fuel cell (SOFC). A lot of research provides a vast knowledge about doping induced exchange bias or exchange bias tuned with doping and doping mediated electronic properties such as half metallicity, band gap, seeback effect, and electronic and ionic conductivity, etc [63, 67–71].

1.8 Motivation

The T_c of LNMO is near room temperature which makes the system useful for different applications. These types of materials also show different kinds of charge, spin, and orbital ordering. The cation ordering and disordering vary with the synthesis route and condition which makes them an interesting candidate to study.

(a) Our objective is to synthesize LNMO by different routes (solid-state and *sol-gel*) to confirm different phase fractions or antisites. The scanning electron microscope (SEM) and transmission electron microscope (TEM) were used to analyze the surface morphology.. To analysis or presence of multiple magnetic transitions confirmed by superconducting quantum interference device (SQUID) magnetometry. The magnetic states across the transition and its nature were defined using SQUID magnetometry in dc/ac field protocols.

(b) The effect of intermediate milling on LNMO structure and magnetism, due to excess surface energy provides during milling and cations mixing will improved. The admixture phase has two T_c due to different magnetic ordering. The low-temperature transition and charge transfer are common in these compounds.

(c) Further, study and synthesis of the Sm doped $La_{2-x}Sm_xNiMnO_6$ (where $x = 0.1$, 0.2, 0.5) by *sol-gel* route. The octahedra tilting induced *via* change in ionic radii, which influence the antisites disorder. The magnetic or spin dynamics of these compound study by magnetization vs temperature and field, ac-susceptibility, and field cooled hysteresis loop measurement.

(d) The spin-glass characteristics and its dynamics explained by frequency dependent ac susceptibility measurement and memory and rejuvenations measurements are done. To confirm exchange bias different field cooled hysteresis loop measurements. The doping and disorder (ASD and APB) influence the exchange interaction.

1.9 Objective of the present thesis

The main objective of this thesis is to synthesis of the LNMO with different routes and investigate the samples to explore the mechnism that how the disorder varies with the synthesis conditions, which we have already discussed based on previous reports. The disorder phase (antisites and APB) varied with the synthesis route and doping. We vary the synthesis route as well as doping (Sm-doped) to check the effect of antisites disorder on magnetism. In this thesis the following objectives will be fulfilled by the following chapter:

• **Chapter 1** presents a literature review about double perovskite, especially LNMO due to its useful properties and characterization. A brief discussion about properties of double perovskites (LNMO) influenced by disorder or cations ordering which is affected by synthesis route and doping.

• **Chapter 2** highlights the synthesis route which is employed to synthesize LNMO nano crystallites. The discussion about characterization techniques to employ surface topology and magnetization measurement by a Superconducting Quantum Interference Device (SQUID) in different protocols.

• **Chapter 3** describes the effect of intermediate milling on LNMO structure and magnetism due to excess surface energy provided during milling. The core-shell structure confirmed by TEM. The magnetic transition varies with milling and provides experimental evidence of charge transfer and two Curie temperatures along different cations ordering.

• **Chapter 4** presents the study and synthesis of the Sm doped $La_{2-x}Sm_xNiMnO_6$ (where x= 0, 0.1, 0.2) by *sol-gel* route. Discussion of synthesis conditions affects the crystal structure. Besides, Sm doping established a single monoclinic phase. This chapter also discuss of spin-glass dynamics and exchange bias varies with Sm doping.

• **Chapter 5** deals with study of spin-glass and exchange bias in sample $La_{1.5}Sm_{0.5}NiMnO_6$. The exchange bias confirms different field hysteresis loop measurements and magnetic training effects. The spin-glass nature also characterizes by memory & rejuvenation and magnetization decay. The Arrot's plot with different modeling confirms the order of magnetic transition.

• **Chapter 6** concludes the major finding of present thesis.

• **Chapter 7** deals with future scope of thesis work that carries significant impact on science and technology. This chapter concludes with future works and suggestions about this system.